NANO · MICRO small
www.small-journal.com

Programmable DNA Nanoindicator-Based Platform for Large-Scale Square Root Logic Biocomputing

Chunyang Zhou, Hongmei Geng, Pengfei Wang, and Chunlei Guo**

The prospect of programming molecular computing systems to realize complex autonomous tasks has advanced the design of synthetic biochemical logic circuits. One way to implement digital and analog integrated circuits is to use noncovalent hybridization and strand displacement reactions in cell-free and enzyme-free nucleic acid systems. To date, DNA-based circuits involving tens of logic gates capable of implementing basic and complex logic functions have been demonstrated experimentally. However, most of these circuits are still incapable of realizing complex mathematical operations, such as square root logic operations, which can only be carried out with 4 bit binary numbers. A high-capacity DNA biocomputing system is demonstrated through the development of a 10 bit square root logic circuit. It can calculate the square root of a 10 bit binary number (within the decimal integer 900) by designing DNA sequences and programming DNA strand displacement reactions. The input signals are optimized through the output feedback to improve performance in more complex logical operations. This study provides a more universal approach for applications in biotechnology and bioengineering.

1. Introduction

Over the past decade, DNA nanotechnology has been used for the development of biocomputing and functional nanodevices, such as molecular diagnostic, smart drug delivery, single molecular analysis, and responsive plasmonic structures.[1–4] For biocomputing, various logic gates based on molecular assemblies[5–7] and organic/inorganic nanomaterials[8,9] have been developed. Among these computing materials, DNA has been considered as an ideal biocomputing substrate since the first demonstration of solving the seven-city Hamiltonian path problem in 1994.[10] The reliable prediction of DNA hybridization reaction based on the Watson–Crick base-pairing principle is indispensable in the construction of biocomputing systems.[11–13] Its simple synthesis method, predictable molecular behavior, and good biocompatibility can largely reduce operating cost, facilitate practical operations in vivo and in vitro, and also provide the potential for the construction of information processing systems.[14] Since George Boole used binary numbers to operate logical operations, assigning "true" to "1" and "false" to "0" in forms of bits, the "Boolean logic computation" was established.[15] Logic gates are basic devices that perform Boolean logic operations, triggered by binary coded inputs (0/1) that produce binary outputs (0/1).[16] However, in biocomputing, the molecular logic gates use binary-encoded molecules as inputs (present as "1" and absence as "0") and optical/electrochemical signals as outputs (high as "1" and low as "0"). Up to now, more basic and advanced biochemical logic gates have been realized, including AND, OR, XOR, NOR, NAND, INHIBIT, encoders, decoders, voters, and keypad locks.[17–20] However, for DNA-based biological computing, the key challenge may be the integration and expansion of logic circuits. On this basis, more complex large-scale logic circuits can be realized, thus promoting the development of DNA computing in various research fields.

In order to develop a desirable and programmable method to realize the large-scale logic circuits, the key mechanism that enables DNA circuits to be rationally programmable is generally based on the powerful DNA hybridization and toehold-mediated DNA strand displacement (TDSD).[21] In particular, the TDSD can dynamically and flexibly manipulate DNA hybridization based on toehold site in a predictable manner,[22–26] which opens up the possibility of coding DNA for large-scale biocomputing. In contrast to previous works,[27a,b,32] most of them are based on the DNA hybridization, the interaction of DNA with nanomaterials, catalytic nucleic acids (DNAzymes)

Dr. C. Y. Zhou, Dr. H. M. Geng, Prof. C. L. Guo
The Guo China-US Photonics Laboratory
Changchun Institute of Optics
Fine Mechanics and Physics
Chinese Academy of Sciences
Changchun, Jilin 130033, China
E-mail: guo@optics.rochester.edu
Dr. C. Y. Zhou, Prof. P. F. Wang
Institute of Molecular Medicine
Renji Hospital
Shanghai Jiao Tong University School of Medicine
Shanghai 200120, China
E-mail: pengfei.wang@sjtu.edu.cn
Dr. C. Y. Zhou, Prof. P. F. Wang
School of Chemistry and Chemical Engineering
Shanghai Jiao Tong University
Shanghai 200120, China
Prof. C. L. Guo
The Institute of Optics
University of Rochester
Rochester, NY 14627, USA
The ORCID identification number(s) for the author(s) of this article can be found under https://doi.org/10.1002/smll.201903489.

DOI: 10.1002/smll.201903489

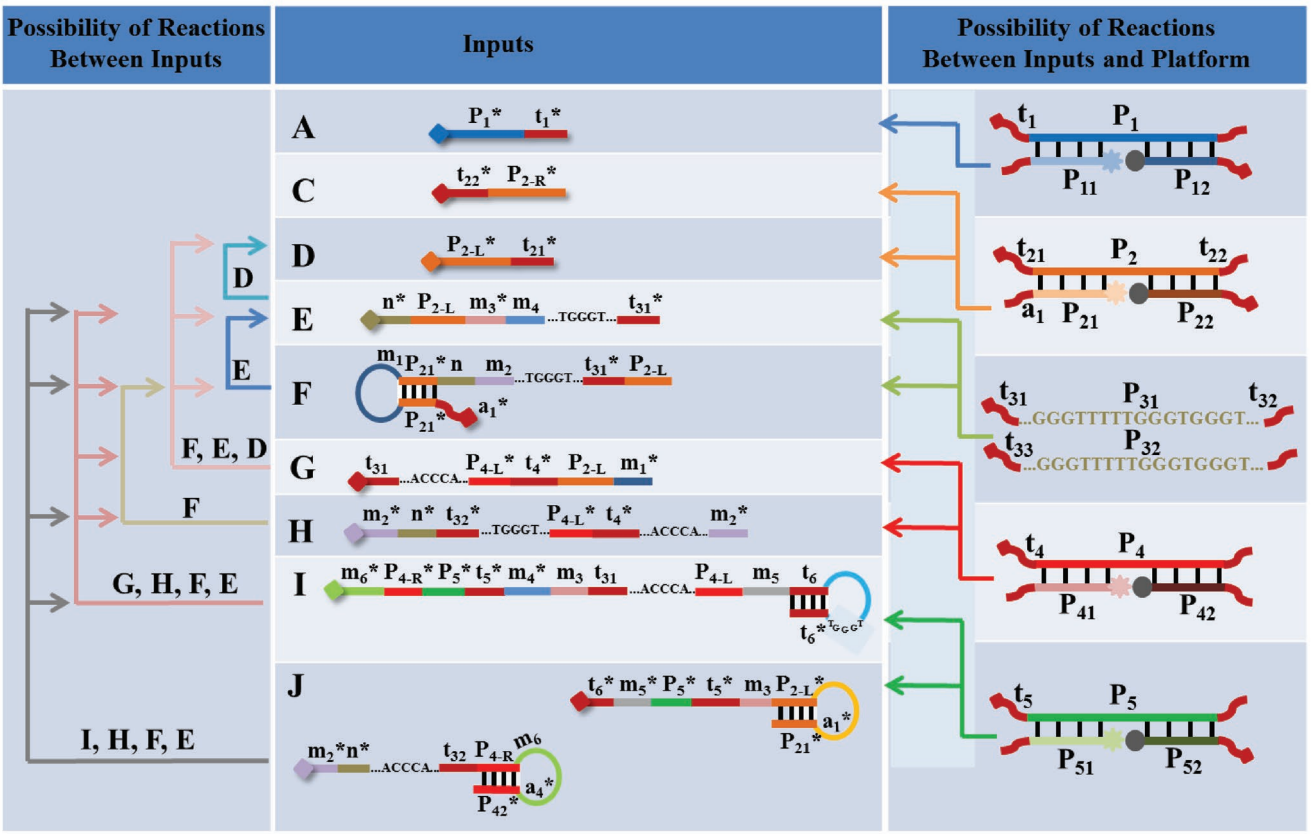

Figure 1. The summary of the possible reactions between the inputs and between inputs and the nanoindicators.

and enzymes to participate in logical operations, which greatly limits the complexity and reaction environment of logical operations. For example, Hu and co-workers developed a novel two-way toehold activation strategy based on the tunable toehold protector on host gold nanoparticles to realize the INH, XOR logic gates, and a half-subtractor.[33] Willner and co-workers have successfully implemented a variety of logic circuits by using libraries of Mg^{2+}-dependent DNAzyme subunits as computational moduli, such as full adder, 2:1 and 4:1 multiplexers and 1:2 demultiplexer.[30,34] Li and co-workers have used three different kinds of enzymes belonging to several classes (i.e., exonuclease, endonuclease, and polymerase) to active or inhibit toehold-mediated DNA strand displacement reaction to many applications including biocomputing and biosensing.[35] In this work, in order to solve this limitation, based on the DNA hybridization, TDSD and the segmentation coding strategy of the input signals, a series of robust and smart nanoindicators are designed (**Figure 1**). These nanoindicators can serve as the reacting platform to construct the large-scale 10 bit square root logic operation, which can calculate the square root of a 10 bit binary number (within the decimal number 900). There are four main reasons to build the nanoindicator-based platform, instead of other indicators, such as hairpin-shaped molecular beacons. First of all, as shown in Figure S1 (Supporting Information), the "four feet protruding" (t_{01}, t_{02}, a_{01}, and a_{02}) nanoindicators are composed of three single-stranded DNAs, and two of them are modified with fluorophore and corresponding quencher. Such designed structures perform a perfect low background signals compare with the hairpin-shaped switches as shown in Figure S1b (Supporting Information). Second, the dissociation of each individual DNA nanoindicator allows distinct displacement reaction to occur in parallel, which is crucial to realizing the large-scale logic circuits. Third, the unique multiple toehold-mediated sites on each nanoindicator greatly improve the programmability and provide more critical and controllable hybridizations for expanding the operation scale of logic circuit. Forth, the introduction of single-stranded DNA with $(GGGT)_3$ as one of the nanoindicators provide stable and controllable fluorescence signal when comes to the DNA with (GGGT) fragment and form the G-quadruple structure (G4). The formation of G4 can be used as an intermediate to interact with *N*-methyl mesoporphyrin IX (NMM, emission max at 609 nm) and enhance its fluorescence intensity.[36,37] This unique structure can cooperate well with other "four feet protruding" nanoindicators and simplify the experiment and reduce the cost, making programming the 10 bit square root logical operation more efficient.

In order to systematic illustrate the operation of 10 bit square root logic circuit, three modular building blocks are built in this work, including the cognitive module, biocomputing module, and definition module. In the "cognitive module," the ten inputs are encoded to recognize one or two specific DNA nanoindicators based on the corresponding toehold-mediated sites (Figure 1). Therefore, the different cognitive inputs can enhance the fluorescence in the nanoindicator, which can be used as an extension of each digit. In the "biocomputing

module," the realization of 10 bit square root logic operation is based on the hybridization reaction between different input combinations and reaction platform, and then different fluorescence signals are obtained as output results. When one or more inputs are combined according to the truth table (**Figure 2**) to calculate the square root of a particular value, two possible kinds of hybridization reactions may occur. The first possibility is the TDSD reactions between the inputs and reaction platform, in which there is no hybridization between the inputs. The second possibility is the inevitable hybridization of the inputs before being added to the reaction platform. By encoding the input sequences, the two possible reactions can be controlled

Radicand	Inputs										Outputs					
	2^9	2^8	2^7	2^6	2^5	2^4	2^3	2^2	2^1	2^0	Y5	Y4	Y3	Y2	Y1	Results
Decimal	J	I	H	G	F	E	D	C	B	A						
1	0	0	0	0	0	0	0	0	0	1	0	0	0	0	1	1
4	0	0	0	0	0	0	0	1	0	0	0	0	0	1	0	2
9	0	0	0	0	0	0	1	0	0	1	0	0	0	1	1	3
16	0	0	0	0	0	1	0	0	0	0	0	0	1	0	0	4
25	0	0	0	0	0	1	1	0	0	1	0	0	1	0	1	5
36	0	0	0	0	1	0	0	1	0	0	0	0	1	1	0	6
49	0	0	0	0	1	1	0	0	0	1	0	0	1	1	1	7
64	0	0	0	1	0	0	0	0	0	0	0	1	0	0	0	8
81	0	0	0	1	0	1	0	0	0	1	0	1	0	0	1	9
100	0	0	0	1	1	0	0	1	0	0	0	1	0	1	0	10
121	0	0	0	1	1	1	1	0	0	1	0	1	0	1	1	11
144	0	0	1	0	0	1	0	0	0	0	0	1	1	0	0	12
169	0	0	1	0	1	0	1	0	0	1	0	1	1	0	1	13
196	0	0	1	1	0	0	0	1	0	0	0	1	1	1	0	14
225	0	0	1	1	1	0	0	0	0	1	0	1	1	1	1	15
256	0	1	0	0	0	0	0	0	0	0	1	0	0	0	0	16
289	0	1	0	0	1	0	0	0	0	1	1	0	0	0	1	17
324	0	1	0	1	0	0	0	1	0	0	1	0	0	1	0	18
361	0	1	0	1	1	0	1	0	0	1	1	0	0	1	1	19
400	0	1	1	0	0	1	0	0	0	0	1	0	1	0	0	20
441	0	1	1	0	1	1	1	0	0	1	1	0	1	0	1	21
484	0	1	1	1	1	0	0	1	0	0	1	0	1	1	0	22
529	1	0	0	0	0	1	0	0	0	1	1	0	1	1	1	23
576	1	0	0	1	0	0	0	0	0	0	1	1	0	0	0	24
625	1	0	0	1	1	1	0	0	0	1	1	1	0	0	1	25
676	1	0	1	0	1	0	0	1	0	0	1	1	0	1	0	26
729	1	0	1	1	0	1	1	0	0	1	1	1	0	1	1	27
784	1	1	0	0	0	1	0	0	0	0	1	1	1	0	0	28
841	1	1	0	1	0	0	1	0	0	1	1	1	1	0	1	29
900	1	1	1	0	0	0	0	1	0	0	1	1	1	1	0	30

Figure 2. The truth table of the 10 bit square root logic operation.

to realize the operation mechanism of the large-scale square root logic operations. After the first two modules are successfully completed, the "definition module" is needed to threshold the outputs by fluorescence signals to showcase the successful operation of the 10 bit square root logic circuit.

2. Results and Discussion

Figure 1 shows the working mechanism for the implementation of the 10 bit square root logic circuit by summarizing the possible reactions between inputs and the interaction between inputs and nanoindicators. First of all, the DNA-based nanoindicator platform is prepared in advance before running the 10 bit square root logic operation. In this work, five kinds of nanoindicators are designed as the reaction platform and are divided into two forms. The first form (P-1, P-2, P-4, and P-5) is a double-stranded DNA structure consisting of three DNA strands and having four "protruding feet," which provide toehold-mediate sites and are programmed to specifically recognize the corresponding input signals. The optimized constructions of the nanoindicators of P-1, P-2, P-4, and P-5 were obtained (details are given in Figures S2 and S3 in the Supporting Information). The second form consists of two single-stranded DNAs with $(GGGT)_3$ segments, which also have four protruding feet and hold the same function as the first form. As shown in Figure 1a, the two single-stranded DNAs with $(GGGT)_3$ segments (P-3-1 and P-3-2) are grouped together and named as P-3. This paper will expound these three modules in depth, reveal the working mechanism and interrelation of each module, and finally realize the successful operation of the 10 bit square root logical operation.

2.1. Cognitive Module

First, in the "cognitive module," each nanoindicator is designed to specifically recognize one or more inputs based on the particular toehold-mediated site. As shown in Figure 1, each input has the priority to hybridize with the corresponding nanoindicator. Some individual input sequences may hybridize with multiple nanoindicators, such as input H, which can hybridize with both P-3 and P-4. However, in order to simplify the programming, it can be summarized as P-4-specific nanoswitch. The concentrations of all inputs have been optimized according to the preoptimized nanoindicator-based reaction platform (details are given in Figure S4 in the Supporting information). Before the addition of inputs to the platform, all the nanoindicators perform very low fluorescence signals due to the close distance between the fluorescence and quenching group, and the fluorescence resonance energy transfer (FRET) occurs (**Figure 3**b, curves a, c, e, g, and i). When the optimized inputs are added to the platform, each of them acts as a switch that lights up the fluorescence signal of the platform. The native polyacrylamide gel electrophoresis (PAGE) experiments (Figure 3c) are performed to further demonstrate the hybridization of the corresponding DNA components in the formation of DNA nanoindicators (detailed explanation is shown in the Supporting Information).

2.2. Biocomputing Module

Second, in the "biocomputing module," we focus on the basic principles of our design in the case of how do inputs interact with each other and with the nanoindicators. First of all, there was no interaction between inputs. When one or more inputs are added to the nanoindicator-based platform, they hybridize directly with the platform according to TDSD and output the corresponding fluorescence signal. The operations that meet this condition include the square root of "1, 4, 9, 16, 36, 64, 144, 256, 576" ($\sqrt[2]{1}=1, \sqrt[2]{4}=2, \sqrt[2]{9}=3, \sqrt[2]{16}=4, \sqrt[2]{36}=6, \sqrt[2]{64}=8, \sqrt[2]{144}=12, \sqrt[2]{256}=16, \sqrt[2]{576}=24$). Second, inputs interact with each other. When more than one inputs are added to the platform according to the truth table (Figure 2), hybridizations may occur preferentially between them instead of the hybridization with platform. In some calculations, different inputs are encoded to inhibit hybridization by other inputs (including inhibiting hybridization with other inputs or with platform, which has been discussed in detail below).

Based on the above programming rules, **Figure 4** summarizes how to implement the 10 bit square root logic computing by classifying the operation range of square root decimal numbers (Figure 4a, $N=1, 1<N\leq 9, 16\leq N\leq 49, 64\leq N\leq 225, 256\leq N\leq 900$). Such classification is based on the nodes that can in turn enhance the five kinds of fluorescence output signals (ranging from Y1 to Y5). First of all, as shown in Figure 4b, the operation is beginning with the square root calculation of the binary number "000 000 0001," which is equal to the decimal positive integer "1" (Figure 4c, curve a1). Second, in order to operate the square root of the decimal numbers within the range of "$1 < N \leq 9$," the binary number "000 000 0100" and "000 000 1001" can be calculated, which is equal to the decimal positive integer "4" and "9." In this case, the input C or inputs D and A are involved according to the truth table (Figure 4c, curve b2, and curves c1 and c2).

The hybridization reaction in the above two calculation ranges belongs to the first case that summarized above, that is, the inputs do not hybridize with each other, but react with the nanodirectors. However, with the expansion of the calculation range, more and more inputs are involved in the logic operation. Therefore, the hybridization reaction in the second case summarized above may occur, that is, the hybridization occurs preferentially between the input DNAs. For example, in the case of operating the square root of the decimal numbers within the range of "$16 \leq N \leq 49$," in order to calculate the square root of "000 001 1001" (decimal positive integer "25"), the inputs A, D, and E are needed. The corresponding desired fluorescently enhanced output signals should be 6-carboxyfluorescein (FAM) and NMM, namely, Y1 and Y3 represent as "high voltage." Therefore, the enhancement of He2+-specific 6-carboxy-X-rhodamine (ROX) fluorescence by input D should be inhibited to make Y2 behaves as a "low voltage." Based on these operational requirements, the input E needs to be encoded, and a sequence fragment (P_{21}) that can hybridize with input D (P_{21}*) can be added to block the TDSD site where D hybridizes with P-2, thus inhibiting the enhancement of ROX (Figure 4c, curve d2).

As the calculation increases to the range of "$64 \leq N \leq 225$," the number of bits of the binary output signal is increased to Y4 (Figure 4b,c). For example, in the case of calculating the square root of "000 111 1001" (decimal positive integer "121"), in order to inhibit the enhancement of output signal Y3 (fluorescence

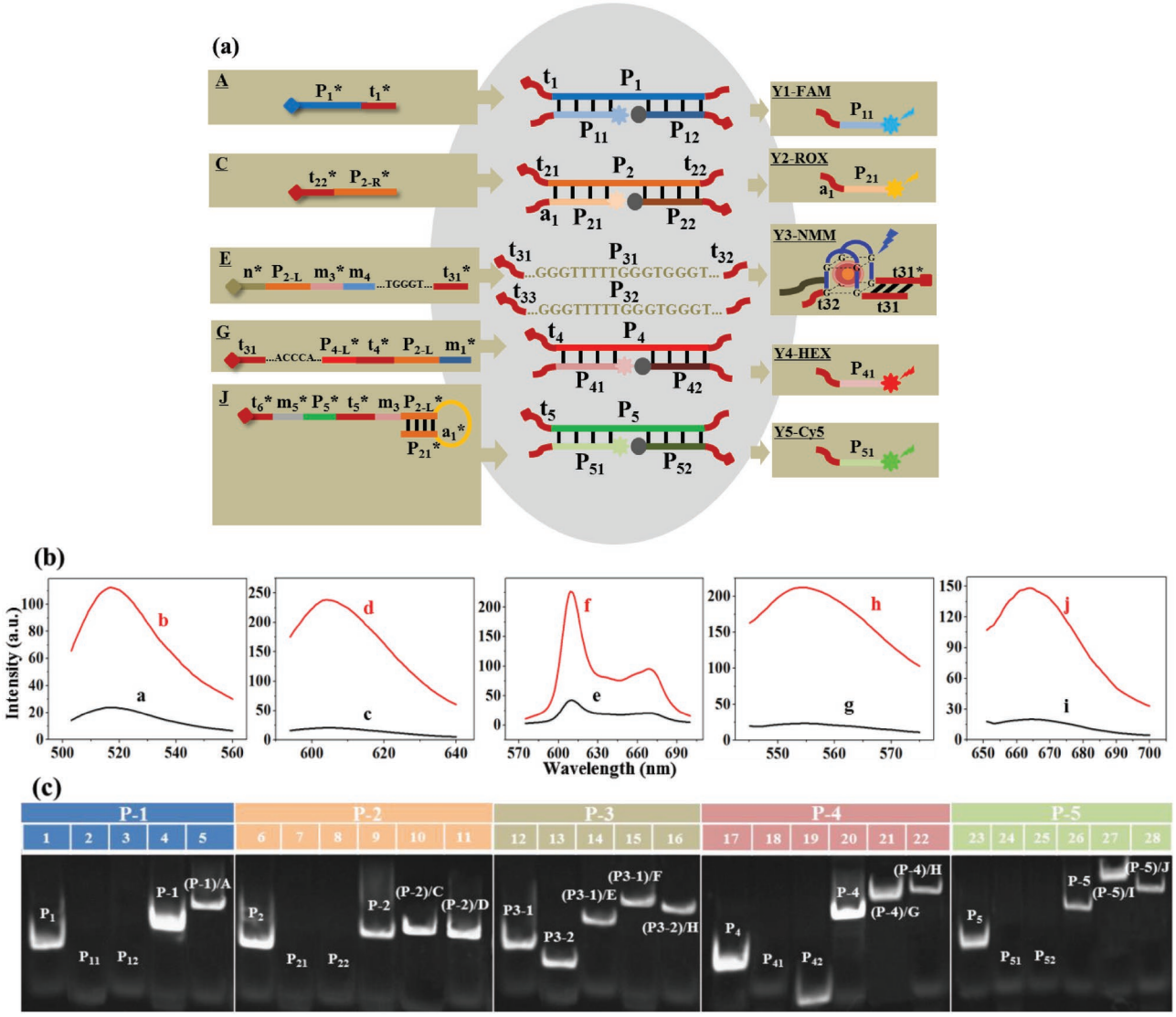

Figure 3. a) The reaction mechanism of the inputs to hybridize with the corresponding nanoindicators. b) The fluorescence intensities of the nanoindicators before and after the inputs are added. c) The native polyacrylamide gel electrophoresis (PAGE) experiments to further demonstrate the hybridization of the corresponding DNA components in the formation of each DNA nanoindicator.

of NMM) induced by inputs E and F, the input G is encoded to add a segment (t_{31}-ACCCA) that can hybridize with the segment of "TGGGT-t_{31}*" in inputs E and F. Therefore, it can block the hybridization sites of inputs E and F to form a G4 structure with P-3, which can lead to the decrease of NMM fluorescence (Figure 4c, curve e3).

Next, as the calculation range extended to "$256 \le N \le 900$," in order to realize the square root operation in this range, a new output signal needs to be extended to Y5. For example, in the case of calculating the square root of "011 110 0100" (decimal positive integer "484"), two coding requirements of the inputs need to be noted. First, in addition to enhancing the fluorescence of hexachlorofluorescein (HEX) to make Y4 perform as "high voltage," input H also need to be encoded to hybridize with P-3 through "t_{32}*-TGGGT" and form the G4 structure, which can lead to the enhancement of NMM fluorescence (Figure 4c, curve f3). Second, in order to inhibit the enhancement of HEX fluorescence induced by inputs G and H, the input I is encoded to add a segment ($P_{4\text{-L}}$) to hybridize with "$P_{4\text{-L}}$*" segment in inputs G and H. Therefore, the sites where hybridization occurred between inputs G and H and P-4 are blocked, and the fluorescence of HEX is inhibited (Figure 4c, curve f4). In the case of calculating the square root of "111 000 0100" (decimal number "900") with the result of "30" (the binary number "11110," $\sqrt[2]{900} = 30$), Y4 is required to perform a "high voltage." Therefore, new coding rules need to be added. At first, the input I is encoded to add a segment of "m_7*-($P_{4\text{-R}}$*)" as shown in Figure 4b. Then, input J-2 is encoded to add a hairpin structure of "($P_{4\text{-R}}$)-m_7-($P_{4\text{-R}}$*)-a_2*." Based on these encoded information, the input I can open the hairpin structure of J-2 through the toehold site of "m7*." At this time, the "($P_{4\text{-R}}$*)-a_2*" fragment is released and can hybridize with P-4, thus making the output Y4 behave as "high voltage" (Figure 4c, curve g4).

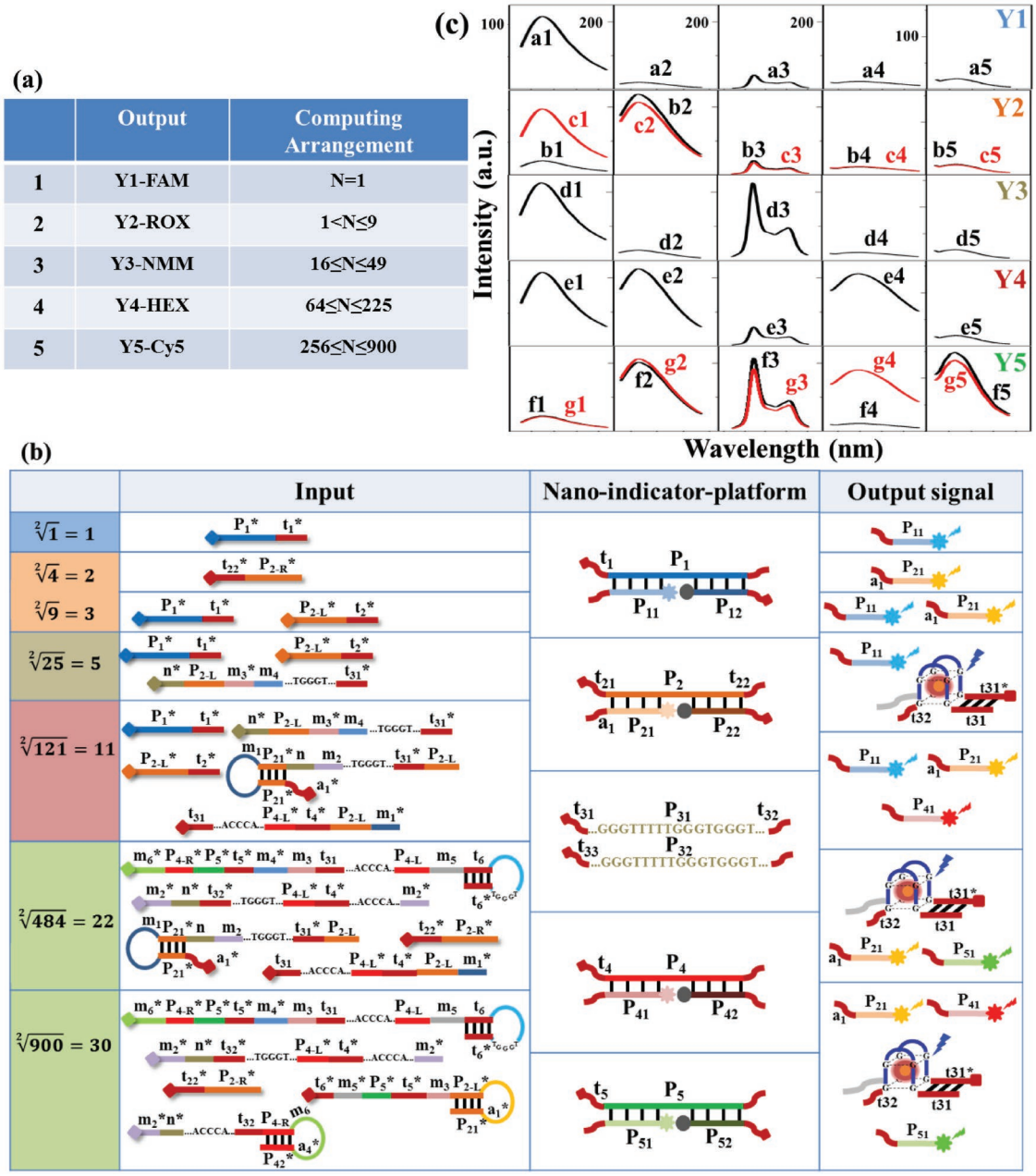

Figure 4. a) The classification of the square root range of computing binary numbers. b) The reaction description of the inputs and nanoindicators to demonstrate the successful operation of 10 bit square root logic circuit during each of the calculation range, which is corresponding to (a).

Based on the DNA nanoindicator platform, the 10 bit square root logic computing has been successfully operated according to the five different fluorescence outputs. Within each calculation range, only a small number of calculations are enumerated in the article, and the other calculation steps to calculate the 10 bit square root logic circuit within the decimal number 900 have been described in detail in Figures S5–S9 (Supporting Information).

2.3. Thresholding Module

Thresholding is actually the digital abstraction of the output signal, namely binarization operation as shown in Figure 1c. It is the basic principle of digital logic in electronics—by pushing essentially analog signals toward ideal ON or OFF value, which is the binary number of "0" or "1."[20] In this work, the **Figure 5** describes the threshold value setting after normalization of the five fluorescence output signals obtained in the 10 bit square root operation. Similar to the approach applies in electronic circuits, the output threshold value is defined as "1" when the normalized fluorescence intensities are higher than 0.5. On the contrary, the output threshold value can be defined as "0" when the normalized fluorescence intensities are lower than 0.5. Because of thresholding, although there may be signal interference in the case of multiple input signals, the output still achieves ideal OFF and ON, and maintains the digital abstraction.

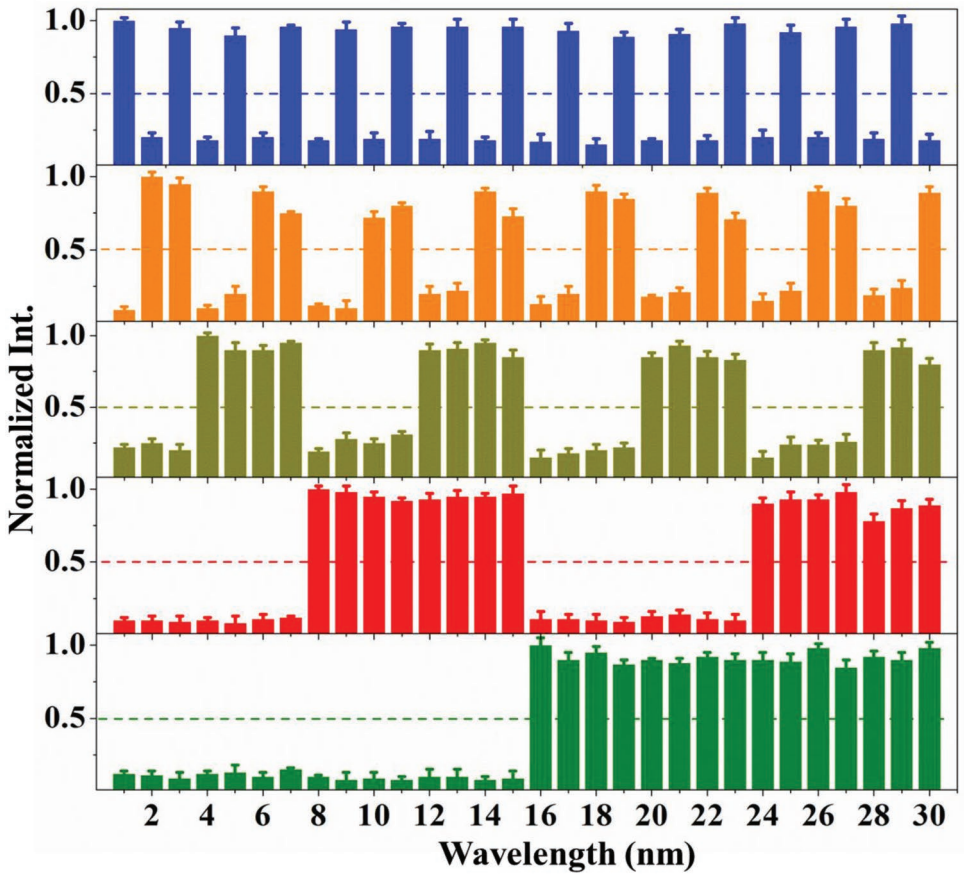

Figure 5. The histogram of the normalized fluorescence intensities of the corresponding reaction platforms. The error bars are obtained via three independent experiments and donate standard deviation (S.D.).

3. Conclusion

In summary, three modules with general principles guided us to successfully realize the complexity of 10 bit square root logic circuit through DNA strand displacement reactions. Cognitive module: First of all, each input is encoded to be classified to recognize specific DNA nanodirector based on the specific toehold-mediated site, which serves as the basis for the implementation of the 10 bit square root logic operation. Biocomputing module: According to the truth table, each cell encodes how the input signals interact with each other and how the input signals react with the nanoindicator-based platform. Finally, the 10 bit square root logical operation is improved. Definition module: The resulting logic output signals need to be threshold, by pushing essentially analog signals toward ideal ON or OFF value, which is the basic principle of digital logic in electronics. Based on these, a series of robust and smart nanoindicators are designed and serve as the reacting platform to construct the 10 bit square root logic operation, which can implement the decimal number within 900 square root operation. Such designed platform performed a perfect low background signals compared with other hairpin-shaped switches. Significantly, the realization of such a relatively large-scale logic system is only based on the predictable DNA strand displacement reaction, which provides a powerful database and a unique structural programmability to DNA to open up inspiring horizons for the designation of novel functional devices and complicated computing circuits. We promise that, in the future, based on the design concept of this work and strong DNA strand displacement reaction to simulate digital or analog signals, and hopefully achieve a wider range of square root calculation, rather than just the square root calculation of integer.

4. Experimental Section

Chemicals and Apparatus: The DNAs used in this work were synthesized by Sangon Biotechnology Company (Shanghai, China) and listed in Table S1 (Supporting Information). All the DNAs were dissolved in distilled water and quantified by Nanodrop One from Thermo with the following extinction coefficients (ε260 nm, M^{-1} cm^{-1}): A = 15 400, G = 11 500, C = 7400, T = 8700. The Acrylamide, ammonium persulfate, Tris (hydroxymethyl) aminomethane, and Boric acid were purchased from Aladdin Biochemical Technology Co. LTD. Ethylene diamine tetraacetic acid (EDTA) was purchased from Sangon Biotechnology Company. NMM was purchased from J&K (Beijing, China). All chemicals used were of analytical reagent without further purification. All solutions were prepared by ultrapure water (18.2 MΩ cm) obtained from Milli-Q purification system. The DNA sequences were dissolved in water as stock solution and diluted with Tris–HCl buffer (20×10^{-3} M Tris–HCl, 200×10^{-3} M KCl, and 10×10^{-3} M $MgCl_2$, pH 8.0) for hybridization in the logic operation. The native polyacrylamide gel electrophoresis

experiments were done by electrophoresis tank from Bio Rad. The gel images were obtained by the BioDoc-It2 Imager from UVP. The fluorescence emission spectra were collected by the Cary Eclipse Fluorescence Spectrophotometer from Agilent Technologies.

Fluorescence Measurement: The fluorescence emission spectra of different samples were collected in Tris–HCl buffer (20×10^{-3} M Tris–HCl, 200×10^{-3} M KCl, and 10×10^{-3} M $MgCl_2$, pH 8.0) at room temperature. The emission spectra of FAM were collected from 500 to 560 nm with the excitation wavelength of 494 nm and slit widths for the excitation and emission were all 5 nm. The emission spectra of ROX were collected from 593 to 640 nm with the excitation wavelength of 585 nm and slit widths for the excitation and emission were all 5 nm. The emission spectra of HEX were collected from 545 to 575 nm with the excitation wavelength of 535 nm and slit widths for the excitation and emission were all 5 nm. The emission spectra of cyanine 5 (Cy5) were collected from 651 to 700 nm with the excitation wavelength of 643 nm and slit widths for the excitation and emission were all 5 nm. For the emission spectra of NMM, they were collected from 575 to 700 nm after excited at 399 nm. The slit widths for the excitation and emission were all 10 nm.

Native Polyacrylamide Gel Electrophoresis: Before use, the DNA stock solutions were diluted to 2×10^{-6} M by Tris–HCl buffer (20×10^{-3} M Tris–HCl, 200×10^{-3} M KCl, and 10×10^{-3} M $MgCl_2$, pH 8.0). After that, they were heated at 90 °C for 10 min and slowly cooled down to room temperature. Then, the desired volume of the platforms and corresponding inputs were added into the mixture to the final volume of 50 µL and incubated for 30 min. After the preparation of 15% native polyacrylamide gel, the electrophoresis was conducted in 1× TBE buffer (17.8×10^{-3} M boric acid, 17.8×10^{-3} M Tris, 2×10^{-3} M EDTA, pH 8.0) at a constant voltage of 100 V for about 1.5 h. Finally, the finished gels were scanned by UV transilluminator.

Statistical Analysis: Before the operation of 10 bit square root logic circuit, the optimized experiments should be done during the hybridization of DNA strands. First of all, the concentrations of the DNA-based nanoindicators, including P-1, P-2, P-3, P-4, and P-5, should be optimized to perform a lower background. The concentrations of the P_1, P_2, P_4, and P_5 were confirmed to be 150×10^{-9}, 175×10^{-9}, 125×10^{-9}, and 150×10^{-9} M, respectively (Figure S2, Supporting Information). The concentrations of P3-1 and P3-2 were all confirmed to be 200×10^{-9} M. Also, the concentrations of P_{11}, P_{21}, P_{41}, and P_{51} were all confirmed to be 125×10^{-9} M, respectively. The optimized concentrations of P_{12}, P_{22}, P_{42}, and P_{52} were confirmed based on the fluorescence intensity of FAM, ROX, HEX, and Cy5 to be 200×10^{-9}, 175×10^{-9}, 225×10^{-9}, and 175×10^{-9} M (Figure S3, Supporting Information). The optimized concentrations of the inputs that involved the hybridization (A, C, D, G, H, I, J) for the operation of 10 bit square root logic circuit were all confirmed to be 175×10^{-9} M, respectively (Figure S4, Supporting Information). The optimized concentrations of inputs E and F were confirmed to be 325×10^{-9} and 275×10^{-9} M (Figure S4, Supporting Information).

Operation of 10 Bit Square Root Logic Circuit: The mixture of optimized nanoindicators (P-1, P-2, P-3, P-4, and P-5) was used as the universal system of all the 10 bit square root logic operation. Different DNA strand solutions were heated at 90 °C for about 10 min and slowly cooled down to room temperature. The operations were performed according to five different calculating ranges ($N = 1$, $1 < N \leq 9$, $16 \leq N \leq 49$, $64 \leq N \leq 225$, $256 \leq N \leq 900$). In order to save the reaction time, cost, and improve the efficiency of calculation, the required different input strands were selected to mix together in advance according to the truth table. Then, the mixture was added into nanoindicator platform-based logic system. The optimized concentrations of inputs and DNA-based nanoindicators were mixed to a final volume of 400 µL and incubated at room temperature. After about 1 h reaction, the fluorescence spectra of FAM, ROX, NMM, HEX, and Cy5 were collected.

Supporting Information

Supporting Information is available from the Wiley Online Library or from the author.

Acknowledgements

This work was supported by the National Key Research and Development Program of China (2017YFB1104700, 2018YFB1107202), The National Natural Science Foundation of China (NSFC, 91750205, 21404015, 61774155, 61705227), and Jilin Science and Technology Department Project (20150204019GX, 20180414019GH).

Conflict of Interest

The authors declare no conflict of interest.

Keywords

DNA hybridization, DNA switching, square root logic circuits, toehold mediated reaction

Received: July 3, 2019
Revised: September 13, 2019
Published online: October 29, 2019

[1] P. W. K. Rothemund, *Nature* **2006**, *440*, 297.
[2] A. Kuzyk, *Nature* **2012**, *483*, 311.
[3] D. Y. Zhang, S. X. Chen, P. Yin, *Nat. Chem.* **2012**, *4*, 208.
[4] Y. Zhang, Z. H. Shuai, H. Zhou, Z. M. Luo, B. Liu, Y. Zhang, L. Zhang, S. F. Chen, J. Chao, L. X. Weng, Q. L. Fan, C. H. Fan, W. Huang, L. H. Wang, *J. Am. Chem. Soc.* **2018**, *140*, 3988.
[5] S. Silvi, E. C. Constable, C. E. Housecroft, J. E. Beves, E. L. Dunphy, M. Tomasulo, F. M. Raymo, A. Credi, *Chem. - Eur. J.* **2009**, *15*, 178.
[6] D. Qu, Q. Wang, H. Tian, *Angew. Chem., Int. Ed.* **2005**, *44*, 5296.
[7] G. d. Ruiter, *J. Mater. Chem.* **2011**, *21*, 17575.
[8] Y. Huang, X. Duan, Y. Cui, L. J. Lauhon, K. H. Kim, C. M. Lieber, *Science* **2001**, *294*, 1313.
[9] C. P. Collier, G. Mattersteig, E. W. Wong, Y. Luo, K. Beverly, J. Sampaio, F. M. Raymo, J. F. Stoddart, J. R. Heath, *Science* **2000**, *289*, 1172.
[10] L. M. Adleman, *Science* **1994**, *266*, 1021.
[11] M. Lin, J. Xu, D. Zhang, Z. Chen, X. Zhang, Z. Cheng, Y. Huang, Y. Li, *J. Theor. Comput. Chem.* **2010**, *332*, 246.
[12] R. J. Lipton, *Science* **1995**, *268*, 542.
[13] M. Rana, E. E. Augspurger, M. S. Hizir, E. Alpa, M. V. Yigit, *J. Mater. Chem. C* **2018**, *6*, 452.
[14] A. K. Geim, K. S. Novoselov, *Nat. Mater.* **2007**, *6*, 183.
[15] A. P. De Silva, S. Uchiyama, *Nat. Nanotechnol.* **2007**, *2*, 399.
[16] D. Q. Fan, E. K. Wang, S. J. Dong, *Mater. Horiz.* **2017**, *4*, 924.
[17] S. L. Xu, H. L. Li, Y. Q. Miao, Y. Q. Liu, E. K. Wang, *NPG Asia Mater.* **2013**, *5*, e76.
[18] M. X. You, L. Peng, N. Shao, L. Q. Zhang, L. P. Qiu, C. Cui, W. H. Tan, *J. Am. Chem. Soc.* **2014**, *136*, 1256.
[19] Z. Z. Huang, H. N. Wang, W. S. Yang, *Nanoscale* **2014**, *6*, 8300.
[20] A. Ogawa, M. Mae da, *Chem. Commun.* **2009**, *31*, 4666.
[21] L. L. Qian, Winfree, E. *Science* **2011**, *332*, 1196.
[22] D. Y. Zhang, E. Winfree, *J. Am. Chem. Soc.* **2009**, *131*, 17303.
[23] Z. Ge, *Anal. Chem.* **2014**, *86*, 2124.
[24] G. Seelig, D. Soloveichik, D. Y. Zhang, Winfree, E. *Science* **2006**, *314*, 1585.
[25] M. G. Zhou, X. G. Liang, T. Mochizuki, H. Asanuma, *Angew. Chem., Int. Ed.* **2010**, *49*, 2167.
[26] F. Lohmann, J. Weigandt, J. Valero, M. Famulok, *Angew. Chem., Int. Ed.* **2014**, *53*, 10372.
[27] C. T. Wu, K. Wang, D. Q. Fan, C. Y. Zhou, Y. Q. Liu, E. K. Wang, *Chem. Commun.* **2015**, *51*, 15940.

[28] C. T. Wu, C. Y. Zhou, E. K. Wang, S. J. Dong, *Nanoscale* **2016**, *8*, 14243.
[29] R. Orbach, S. Lilienthal, M. Klein, R. D. Levine, F. Remacle, I. Willner, *Chem. Sci.* **2015**, *6*, 1288.
[30] R. Orbach, R. D. Levine, F. Remacle, I. Willner, *Chem. Sci.* **2014**, *5*, 1074.
[31] D. Q. Fan, C. S. Shang, W. L. Gu, E. K. Wang, S. J. Dong, *ACS Appl. Mater. Interfaces* **2017**, *9*, 25870.
[32] C. Y. Zhou, K. Wang, D. Q. Fan, C. T. Wu, D. L. Liu, Y. Q. Liu, E. K. Wang, *Chem. Commun.* **2015**, *51*, 10284.
[33] Y. Z. Liu, B. R. Dong, Z. T. Wu, W. Fang, G. H. Zhou, A. G. Shen, X. D. Zhou, J. M. Hu, *Chem. Commun.* **2014**, *50*, 12026.
[34] R. Orbach, F. Wang, O. Lioubashevski, R. D. Levine, F. Remacle, I. Willner, *Chem. Sci.* **2014**, *5*, 3381.
[35] C. Li, L. Shi, Y. Q. Tao, X. X. Mao, Y. Xiang, G. X. Li, *Sci. Rep.* **2017**, *7*, 10017.
[36] C. Y. Zhou, D. L. Liu, S. J. Dong, *ACS Appl. Mater. Interfaces* **2016**, *8*, 20849.
[37] C. Y. Zhou, H. M. Geng, C. L. Guo, *Acta Biomater.* **2018**, *80*, 58.

